ARTICLES

Collision-Induced Dissociation of II−VI Semiconductor Nanocrystal Precursors, Cd^{2+} and Zn^{2+} Complexes with Trioctylphosphine Oxide, Sulfide, and Selenide

Won Ja Min, Sunghan Jung, Sung Jun Lim, Yongwook Kim, and Seung Koo Shin*

Bio-Nanotechnology Center, Department of Chemistry, Pohang University of Science and Technology, San 31 Hyoja-dong Namgu, Pohang, Kyungbuk 790-784, Korea

Received: June 2, 2009; Revised Manuscript Received: July 17, 2009

The metal (M = Cd^{2+} and Zn^{2+}) complexes with trioctylphosphine chalcogenide (TOPE, E = O, S, and Se) are prepared by electrospray ionization, and their relative stabilities and intramolecular reactions are studied by collision-induced dissociation (CID) with Xe under single collision conditions. These metal−TOPE complexes are considered as molecular precursors for the colloidal synthesis of II−VI compound semiconductor nanocrystals employing TOPO as a metal-coordinating solvent and TOPS or TOPSe as a chalcogen precursor. Of the various $[M + nTOPE]^{2+}$ ($n = 2-7$) ions generated by ESI, the $n = 2-4$ complexes are characterized by CID as a function of collision energy. The collision energy at 50% dissociation ($E_{50\%}$) is determined from the cracking curve and the relative stabilities of the complexes are established. Between the two metal ions, the zinc−TOPE complexes are more stable than the cadmium−TOPE complexes when $n = 2-3$, whereas their stabilities are reversed when $n = 4$. Of the TOPE, TOPO binds most strongly to the metal ion, while TOPSe does most weakly. Upon CID, loss of TOPE occurs exclusively from the tetra-TOPE complexes, while extensive fragmentation of TOPE takes place from the di-TOPE complexes, showing the signature of the metal chacogenide formation. The nucleation of nanocrystals appears to begin with cracking of $[M + 2TOPE]^{2+}$ (E = S and Se).

Introduction

II−VI compound semiconductor nanocrystals have emerged as novel fluorophores in optoelectronic[1,2] and biological applications[3−5] because of their high photostability, narrow emission from broad excitation wavelengths, and size-tunable luminescence. Of the II−VI materials, CdSe emitting in the visible-wavelength region has been most widely used as core materials,[6−11] while CdS, ZnS, and ZnSe with larger bandgaps than CdSe have been used as shell materials to protect, modify, and/or enhance the optical properties of CdSe core nanocrystals.[12−20] These core and core/shell structure nanocrystals have been typically produced by colloidal synthesis at high temperature employing either a coordinating solvent like trioctylphosphine oxide (TOPO)[6−9,12−18] or a noncoordinating solvent like 1-octadecene.[10,11,19,20] Trioctylphosphine sulfide (TOPS) and trioctylphosphine selenide (TOPSe) are often used as chalcogen precursors.[6,8,9,12−19] Although much progress has been made in controlling the crystal lattice,[8−11] size,[6−11] shape,[21−24] and composition[25−27] of the II−VI metal−chalcogen nanocrystals, not much is known about the relative stabilities of the metal-TOPE (E = O, S, and Se) complexes formed at the very beginning of synthesis. Most of the spectroscopic studies using NMR and UV/vis absorption/emission carried out in solution have dealt with an ensemble average of heterogeneous nanocrystals grown at various rates. To be more specific about the interaction between the metal ion and chalcogen-containing ligands, we need to employ a molecular probe that is not only selective toward the specific complex of interest but also capable of inducing chemical reactions at elevated energies. Electrospray ionization (ESI) offers a reproducible means to bring the complex ions present in solution into the gas phase,[28−31] and mass spectrometry (MS) enables the cracking of the mass-selected complex ions in the absence of solvent and counterions.[32−35]

In this report, we have employed ESI-MS to prepare the metal−TOPE complex ions with varying degrees of the coordination number and examined their cracking patterns as a function of collision energy. Collision with Xe under single-collision conditions imparts the center-of-mass collision energy into the vibrational degrees of freedom, thus elevating the internal energy of the complex ion. The energy-dependent cracking patterns provide the relative stabilities of the metal−TOPE complexes and reveal the intramolecular reactions that lead to the formation of metal chalcogenide.

We have prepared the $[M + nTOPE]^{2+}$ complex ions (M = Cd and Zn, E = O, S, and Se, $n = 2-4$) by ESI of a mixture of metal nitrate or acetate and TOPE in a 2:1 (v/v) acetone/methanol solution and carried out collision-induced dissociation (CID) of the complex ions using a quadrupole time-of-flight (Q-TOF) mass spectrometer. The collision energy that leads to 50% dissociation of the complex ion ($E_{50\%}$) is determined from the CID yield-energy curve. For each coordination number n, all $[M + nTOPE]^{2+}$ complex ions (M = Cd and Zn, E = O, S, and Se) have the same number of degrees of freedom (DOF), thus values of $E_{50\%}$ can be used without DOF correction to compare the relative

* Corresponding author. Tel: (+82) 54 279 2123. Fax: (+82) 54 279 3399. E-mail: skshin@postech.ac.kr.

10.1021/jp905153v CCC: $40.75
Published on Web 08/06/2009

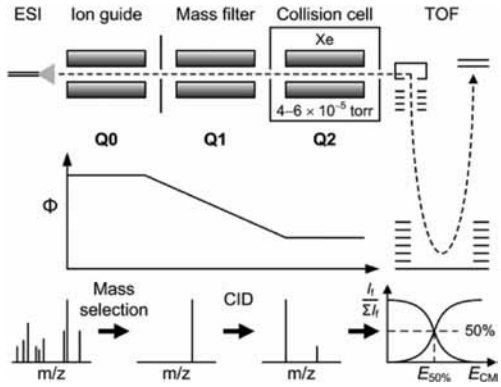

Figure 1. Schematic of an experimental setup.

stabilities of the complex ions.[32,35] Although $E_{50\%}$ is not threshold energy, it is a measure of the total binding energy of the complex ion. Especially, when both the binding and dissociation modes are identical as in [M + nTOPE]$^{2+}$ complexes, the relative stabilities can be established with $E_{50\%}$ values.[32−35] CID results show that [M + 4TOPE]$^{2+}$ dissociates exclusively to [M + 3TOPE]$^{2+}$ with a loss of TOPE for both Cd and Zn, while [M + 2TOPE]$^{2+}$ undergoes extensive fragmentations indicating the formation of metal chalcogenide. The present results shed light on the molecular basis of the metal chalcogenide formation at the very beginning of TOPO-based colloidal synthesis of II−VI compound semiconductor nanocrystals.

Experimental Section

Chemicals. $Cd(NO_3)_2 \cdot 4H_2O$ (99.999%), $Zn(NO_3)_2 \cdot xH_2O$ (99.999%), $Zn(CH_3COO)_2$ (99.99%), TOPO (99%), TOP (technical grade, 90%), sulfur powder (99.998%), and selenium power (100 mesh, 99.99%) were purchased from Sigma-Aldrich (St. Louis, MO). HPLC-grade methanol and acetone were obtained from J. T. Baker (Phillipsburg, NJ). TOP was purified by distillation, but other chemicals were used without further purification.

ESI Sample Preparation. For the metal−TOPO complexes, cadmium nitrate or zinc nitrate (0.30 mg) was mixed with TOPO (0.38 mg) in methanol (10 mL). TOPS and TOPSe was prepared by slowly heating up a TOP solution containing an excess amount of sulfur or selenium powder under nitrogen pressure. For the cadmium−TOPS and TOPSe complexes, cadmium nitrate (0.3 mg) was mixed with TOPS or TOPSe (0.3 μL) in a 2:1 (v/v) acetone/methanol solution (10 mL) degassed by freeze−pump−thaw. For the zinc−TOPS and TOPSe complexes, zinc acetate (0.18 mg) was mixed with TOPS or TOPSe (0.3 μL) in a 2:1 acetone/methanol or 1:1 ethanol/methanol solution degassed by freeze−pump−thaw.

Collision Induced Dissociation (CID). A schematic of an experimental setup is shown in Figure 1. A triple quadrupole time-of-flight (Q-TOF) mass spectrometer (QSTAR Pulsar-i, Applied Biosystems, Concord, Canada) was equipped with a turbo electrospray ionization source. Ions were sprayed at 4 kV with a flow rate of 5 μL/min, collimated at the first quadrupole (Q0), mass-selected at the second quadruple (Q1), and undergone CID at the third quadruple (Q2) inside a collision cell. The partial pressure of Xe in the collision cell was kept at (4−6) × 10^{-5} Torr and the background pressure was kept below 1 × 10^{-5} Torr. On average, two-thirds of ions were supposed to undergo at least one collision with Xe at thermal energy. Fragment ions were analyzed using an orthogonal reflectron-type TOF detector. The CID spectra were acquired as a function of collision energy by varying the voltage between Q0 and Q2. The relative abundances of the parent and fragment ions were plotted as a function of collision energy in the center-of-mass

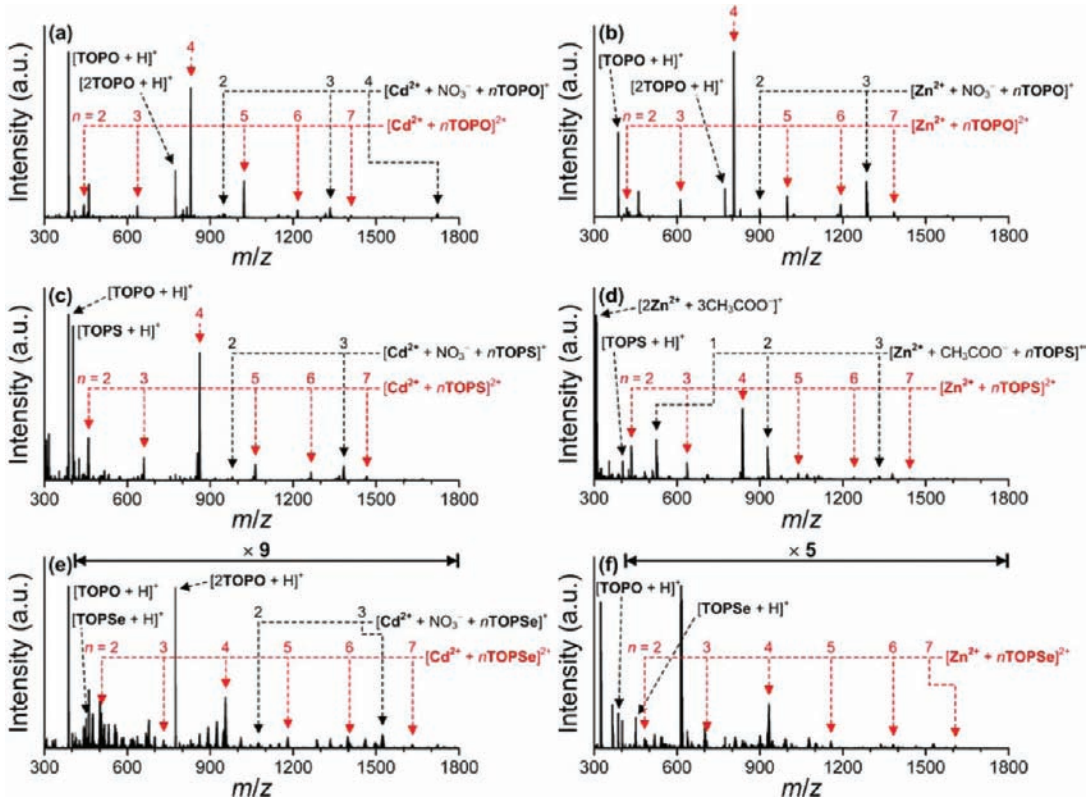

Figure 2. ESI mass spectra of the mixture of metal nitrate or acetate and TOPE: (a) $Cd(NO_3)_2$ + TOPO; (b) $Zn(NO_3)_2$ + TOPO; (c) $Cd(NO_3)_2$ + TOPS; (d) $Zn(CH_3COO)_2$ + TOPS; (e) $Cd(NO_3)_2$ + TOPSe; (f) $Zn(CH_3COO)_2$ + TOPSe.

frame (E_{CM}). The collision energy in the center-of-mass frame, E_{CM}, is given in eq 1.

$$E_{CM} = \left(\frac{m_{Xe}}{m_{ion} + m_{Xe}}\right)E_{lab} \quad (1)$$

where m_{Xe} is the mass of Xe, m_{ion} is the mass of the incoming ion, and E_{lab} is the kinetic energy of an ion in the laboratory frame, which is the sum of the initial kinetic energy acquired in the ion source region and the gain in potential energy by the voltage difference between Q0 and Q2. The natural abundances of Xe isotopes are taken into account in the average collision energy as expressed in eq 2.

$$E_{CM} = \sum_j P_j\left(\frac{m_{Xe_j}}{m_{ion} + m_{Xe_j}}\right)E_{lab} \quad (2)$$

where P_j is the population of the jth isotope of Xe. The spread in natural isotopes contributes ±3.2% of an error in average collision energy.

The initial kinetic energy of an ion along the quadrupole axis was calculated from the flight time of an ion through the orthogonal TOF analyzer and the center-to-center distance (15 cm) between an ion pusher and an MCP detector after applying the same voltage to both Q0 and Q2. Because all ions were accelerated into the ion pusher of the TOF analyzer by an offset voltage V_{off} (either 9.46 or 9.60 V depending on instrument tuning conditions), the initial kinetic energy was obtained by subtracting the gain in potential energy due to V_{off} from the axial kinetic energy. The initial kinetic energy acquired in the source region was determined to be 10.62 ± 0.04 eV for the 2+ ion independent of mass. The spread in initial kinetic energy also contributed to an error in collision energy.

Results and Discussion

Complexes of Cd^{2+} and Zn^{2+} with TOPE (E = O, S, and Se). ESI yields $[M + nTOPE]^{2+}$ complexes with $n = 2-7$ as displayed in Figure 2. Higher-order complexes ($n > 7$) are observed in trace amounts. The ESI mass spectra also show the nitrate- or acetate-containing metal−TOPE complexes, $[M^{2+} + NO_3^- + mTOPE]^+$ with $m = 2-4$ or $[M^{2+} + CH_3COO^- + mTOPE]^+$ with $m = 1-3$. In addition, the protonated TOPE species, such as $[TOPO + H]^+$, $[TOPS + H]^+$, $[TOPSe + H]^+$, and $[2TOPO + H]^+$, appear prominent. The mixture of TOP with sulfur or selenium powder always yields $[TOPO + H]^+$ due to oxygen uptake by TOP during ESI sample loading. Of the $[M + nTOPE]^{2+}$ complexes, the tetra-TOPE complexes are most intense, suggesting the magic number of four for the TOPE coordination on the d^{10} metal ion. The VSEPR theory predicts a linear, equilateral triangle, and tetrahedral geometry for the di-, tri- and tetra-TOPE coordination complex, respectively.[36] Higher-order coordination complexes with $n \geq 5$ are considered to have each additional TOPE on the faces of tetrahedron. The geometry of the coordination complex is presented in Figure 3. The ionic radii of metal ions, atomic radii of chalcogens, and average P═E bond distances are also given.[37] The cone angle of TOP is estimated at 130°.[37] The binding of nitrate or acetate on the metal ion results in the reduction of the number of TOPE coordination, presumably due to the decrease in net charge on the metal from +2 to +1.

Collision-Induced Dissociation of $[M + nTOPE]^{2+}$ Complexes ($n = 2-4$). Of the various complex ions, $[M + nTOPE]^{2+}$ with $n = 2-4$ are characterized by CID. In cases of $[M + 2TOPO]^{2+}$ and $[Zn + 2TOPSe]^{2+}$, where the peaks are weak and congested, CID fails to provide any meaningful data. Higher-order complexes with $n \geq 5$ undergo loss of TOPE at very low collision energy (data not shown), indicating that TOPE on the face of tetrahedron is weakly bound. The CID yield-energy curve plotting the relative abundance of the parent ion as a function of collision energy is presented in Figure 4. For both metal ions, as the TOPE-coordination number increases from $n = 2$ to 3 and 4, the CID curve shifts to lower and lower energy. Among TOPE, TOPO yields the cracking curve at the highest energy range, while TOPSe results in the curve at the lowest energy range. Between the two metal ions, Zn^{2+} needs more energy than Cd^{2+} when $n = 2$ and 3, but slightly less energy when $n = 4$. For di- and tri-TOPE complexes with the coordinatively unsaturated metal center, the TOP cones provide little steric hindrance on linear or equilateral triangle geometry (Figure 3). Thus, TOPE binds more strongly to Zn^{2+} than Cd^{2+} because chalcogens get closer to the smaller metal ion than the larger one. On the other hand, for tetra-TOPE complexes with the coordinatively saturated metal center, the TOP cones on the apex of tetrahedron (Figure 3) exert more steric hindrance as chacogens get closer to the metal center. Consequently, the binding of TOPE on Zn^{2+} are sterically more hindered than that on Cd^{2+}, thus resulting in a weaker TOPE binding to zinc than to cadmium.

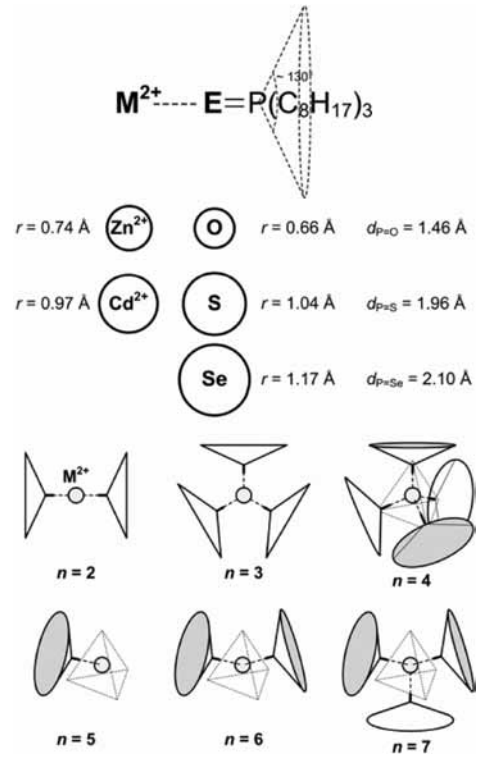

Figure 3. Geometries of the metal−TOPE coordination complexes. The ionic radii of the metal ions and the atomic radii of chalcogens are taken from ref 36; the phosphine−chalcogen distances in TOPE are taken from ref 37. The phosphine cone angle is estimated from the values listed in ref 37.

Intramolecular Reactions of $[M + nTOPE]^{2+}$ Complexes ($n = 2-3$). Collision activates intramolecular reactions of $[M + nTOPE]^{2+}$ complexes for $n = 2-3$. The relative abundance of CID fragments is plotted in Figure 5 for the tri-TOPE complexes as a function of collision energy. In the case of TOPO (Figure 5a,b), as the collision energy increases, $[TOPO + H]^+$

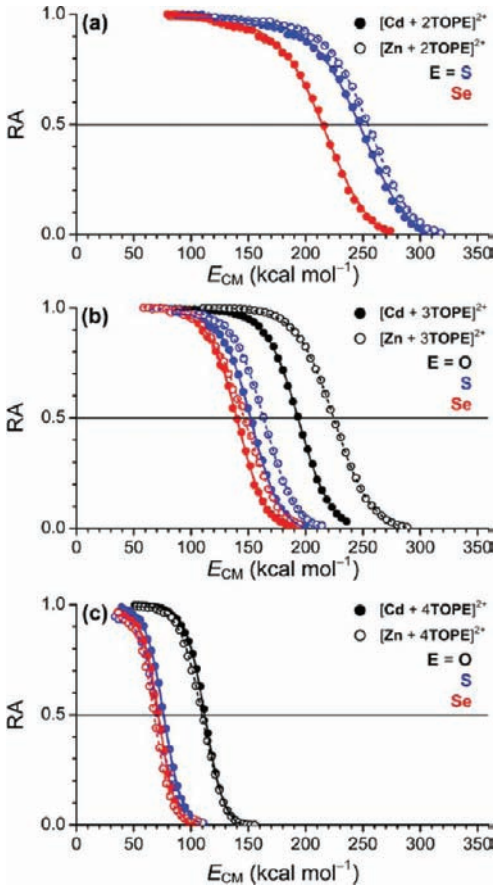

Figure 4. CID yield-energy curve of the [M + nTOPE]$^{2+}$ complex presenting the relative abundance (RA) of the parent ion as a function of the center-of-mass (CM) collision energy E_{CM} in units of kcal mol^{-1}: (a) $n = 2$; (b) $n = 3$; (c) $n = 4$.

arises before the appearance of [M + 2TOPO]$^{2+}$ for both metal ions. At high energy, [M + 2TOPO]$^{2+}$ dissociates to [TOPO + H]$^+$ and [M + TOPO′ + H]$^+$ as well as [TOPO′ + H]$^+$ and [M + TOPO + H]$^+$, where the prime denotes dehydrogenated TOPO, thus TOPO′ representing [TOPO − H_2].[38] [TOPO′ + H]$^+$ dissociates further to [DOPO′ + H]$^+$ by loss of C_8H_{16}, where DOPO′ refers dehydrogenated dioctylphosphine oxide, [DOPO − H_2]. Interestingly, both [MO + TOPO + H]$^+$ and [TOP′ + H]$^+$ peaks appear at very high energy for both metal ions, indicating the P═O bond cleavage with the concomitant formation of metal oxide. In the case of TOPS (Figure 5c,d), the TOPS-loss product, [M + 2TOPS]$^{2+}$, occurs first for both metal ions, and then [TOPS + H]$^+$ appears second followed by other fragments. Similarly to the TOPO complexes, [M + 2TOPS]$^{2+}$ subsequently dissociates to [TOPS + H]$^+$ and [M + TOPS′ + H]$^+$ as well as [TOPS′ + H]$^+$ and [M + TOPS + H]$^+$, and [TOPS′ + H]$^+$ dissociates further to [DOPS′ + H]$^+$. In the case of TOPSe (Figure 5e and 5f), the fragmentation patterns are somewhat different from the other two cases. The loss of TOPSe occurs almost exclusively at collision energy below $E_{50\%}$. [TOPSe′ + H]$^+$, [DOPSe′ + H]$^+$, and MOPSe$^{+\bullet}$ appear in trace amounts at collision energy above $E_{50\%}$. MOPSe$^{+\bullet}$ refers the radical cation of octylphosphine selenide. Apparently, intramolecular reactions take place more readily when the metal-TOPE binding is strong.

Collision-activated intramolecular reactions are more prominent in the di-TOPE complexes as displayed in Figure 6. In cases of [Cd + 2TOPS]$^{2+}$, [Zn + 2TOPS]$^{2+}$, and [Cd + 2TOPSe]$^{2+}$ complexes, loss of TOPE is not observed in the entire energy range. With TOPS, the primary dissociation products are [TOPS + H]$^+$ and [M + TOPS′ + H]$^+$, [TOPS′ + H]$^+$ and [M + TOPS + H]$^+$, and [DOPS′ + H]$^+$, similarly to [M + 3TOPO]$^{2+}$. More importantly, [MS + TOPS + H]$^+$ and [TOP′ + H]$^+$ appear in trace amounts at high energy for both metal ions, suggesting the cleavage of P═S bond with the formation of metal-sulfide bond. With TOPSe, [TOPSe′ + H]$^+$, [DOPSe′ + H]$^+$, and MOPSe$^{+\bullet}$ appear prominently, but both the [Cd + TOPSe′ + H]$^+$ and [Cd + TOPSe + H]$^+$ ions are not observed. However, similarly to the di-TOPS complexes, [CdSe + TOPSe + H]$^+$ and [TOP′ + H]$^+$ appear at high energy, providing evidence for the formation of cadmium selenide.

Relative Stabilities of [M + nTOPE]$^{2+}$ Complexes (n = 2−4). In cases of [M + 4TOPE]$^{2+}$, [M + 3TOPS]$^{2+}$, and [M + 3TOPSe]$^{2+}$, where the primary dissociation channel involves exclusive loss of TOPE, $E_{50\%}$ is considered as a relative measure of the metal−chalcogen binding energy. On the other hand, In cases of [M + 3TOPO]$^{2+}$, [M + 2TOPS]$^{2+}$, and [Cd + 2TOPSe]$^{2+}$, where the primary dissociation channels involve intramolecular reactions, $E_{50\%}$ is considered a lower limit. Values of $E_{50\%}$ are listed in Table 1 and plotted in Figure 7 as a function of chalcogen atomic radius. As the coordination number n increases from 2 to 3 and 4, $E_{50\%}$ decreases by sizable increments for both metal ions. As the chalcogen atomic radius increases, $E_{50\%}$ decreases by small decrements for both metal ions. The descending slope gets increasingly steep as the coordination numbers decrease. Of the TOPEs, TOPO is the most strongly coordinating ligand, whereas TOPSe is the most weakly coordinating ligand. The coordinating power of TOPS is closer to TOPSe than TOPO because the atomic radius of sulfur is closer to that of selenium.

Mechanisms of Intramolecular Reactions. The coordinatively unsaturated metal−TOPE complexes (n = 2−3) have yielded a number of intramolecular reaction products. There are some common features as listed in eq 3−8.

$$[M + 4TOPE]^{2+} \rightarrow [M + 3TOPE]^{2+} + TOPE \quad (3)$$

$$[M + 3TOPE]^{2+} \rightarrow [M + 2TOPE]^{2+} + TOPE \quad (4)$$

$$\rightarrow [TOPE + H]^+ + [M + TOPE + TOPE' + H]^+ \quad (5)$$

$$[M + 2TOPE]^{2+} \rightarrow [M + TOPE' + H]^+ + [TOPE + H]^+ \quad (6)$$

$$\rightarrow [M + TOPE + H]^+ + [TOPE' + H]^+ \quad (7)$$

$$\rightarrow [ME + TOPE + H]^+ + [TOP' + H]^+ \quad (8)$$

The loss of TOPE occurs exclusively over the entire energy range in the tetra-TOPE complexes (reaction 3). For the tri-TOPE complexes, the loss of TOPE takes place exclusively at low energy (reaction 4) with TOPS and TOPSe, but the [TOPE + H]$^+$ channel becomes competitive when the metal-TOPE binding is strong, as in the tri-TOPO and -TOPS complexes (reaction 5). In cases of the di-TOPE complexes, the occurrence of intramolecular reactions prevents the loss of TOPE (reactions 6−8). The mechanism of intramolecular rearrangements is proposed in Scheme 1. The mechanisms presented in Scheme 1a,b involve hydride transfer from one CH_2 moiety in the octyl group to the metal ion[38] and concurrent proton transfer from

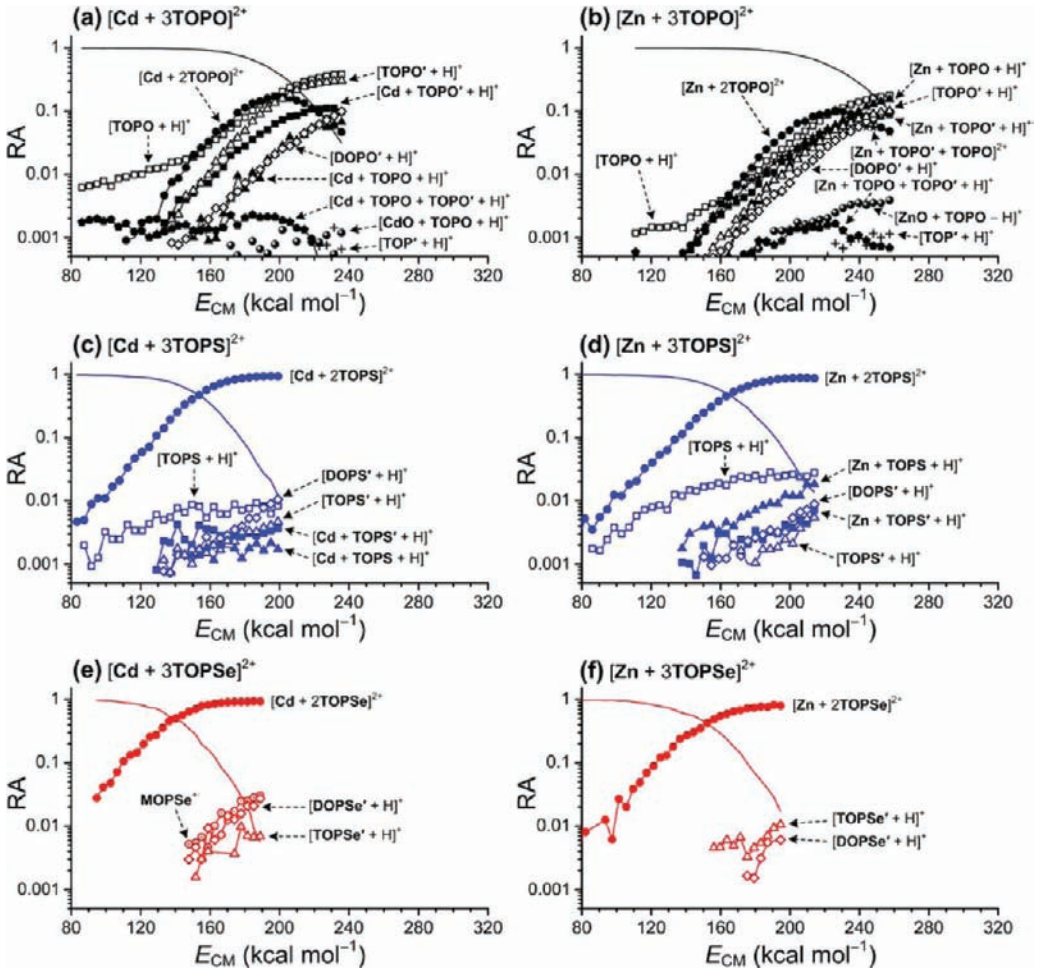

Figure 5. Relative abundance (RA) of the parent (solid line) and daughter ions (symbols) from CID of $[M + 3TOPE]^{2+}$ as a function of the center-of-mass (CM) collision energy E_{CM} in units of kcal mol^{-1}: (a) $[Cd + 3TOPO]^{2+}$; (b) $[Zn + 3TOPO]^{2+}$; (c) $[Cd + 3TOPS]^{2+}$; (d) $[Zn + 3TOPS]^{2+}$; (e) $[Cd + 3TOPSe]^{2+}$; (f) $[Zn + 3TOPSe]^{2+}$.

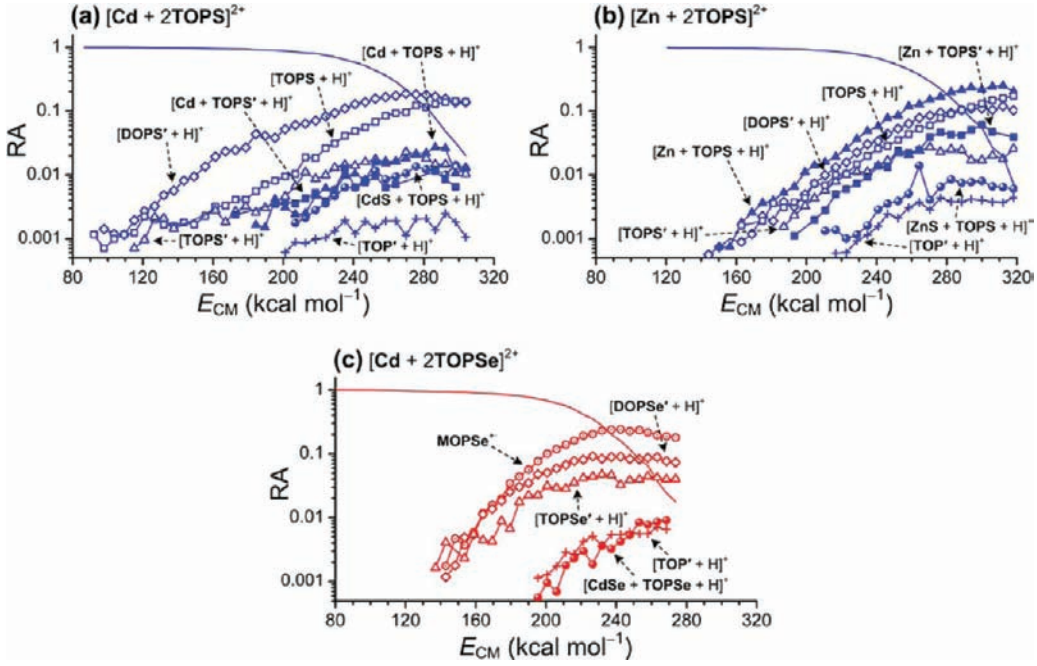

Figure 6. Relative abundance (RA) of the parent (solid line) and daughter ions (symbols) from CID of $[M + 2TOPE]^{2+}$ as a function of the center-of-mass (CM) collision energy E_{CM} in units of kcal mol^{-1}: (a) $[Cd + 2TOPS]^{2+}$; (b) $[Zn + 2TOPS]^{2+}$; (c) $[Cd + 2TOPSe]^{2+}$.

adjacent CH_2 to the chalcogen atom, which leaves a carbon−carbon double bond behind. Reaction 4 (Scheme 1a) results in proton transfer to the chalcogen atom on the other TOPE, thus releasing $[TOPE + H]^+$. On the other hand, reaction 7 (Scheme

TABLE 1: $E_{50\%}$ Values of [M + nTOPE]$^{2+}$ (kcal mol^{-1})[a]

		TOPE		
M^{2+}	n	E = O	E = S	E = Se
Cd^{2+}	2		247 ± 8[b]	214 ± 7[b]
	3	193 ± 6[b]	152 ± 5	140 ± 5
	4	112 ± 4	76 ± 3	72 ± 2
Zn^{2+}	2		254 ± 8[b]	
	3	224 ± 7[b]	163 ± 5	146 ± 5
	4	109 ± 4	71 ± 2	68 ± 2

[a] Errors are from the Xe isotope distribution and the curve fitting. [b] A lower limit.

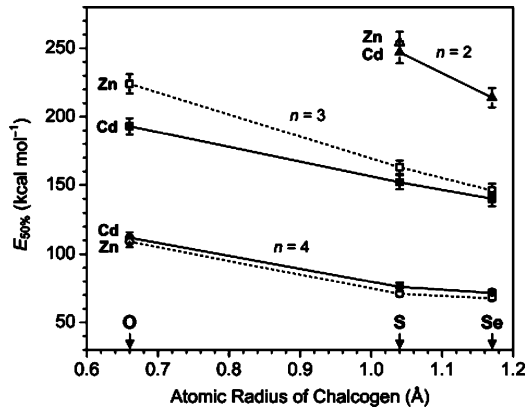

Figure 7. $E_{50\%}$ values as a function of chalcogen atomic radius.

1b) results in proton transfer to the chalcogen atom of its own TOPE to which the reactive octyl group belongs, thus releasing [TOPE′ + H]$^+$. Reaction 8 (Scheme 1c) involves electron transfer from an electron-rich P = E bond to the electron-deficient metal ion, which leads to the formation of M−E and P−E bonds with metal-to-phosphorus charge transfer. Then one of the alkyl groups in activated TOPE undergoes hydride transfer to P$^+$, concomitant proton transfer to the chalcogen atom, and electron transfer from P−E to M−E bonds, which leads to the P−E bond cleavage and the metal−chalcogen bond formation. In the case of the [Cd + 2TOPSe]$^{2+}$ complex, it seems that intramolecular reaction 7 (Scheme 1b) takes place twice (either in sequence or in parallel) to form 2[TOPSe′ + H]$^+$ with loss of neutral cadmium dihydride (Scheme 1d). Of the reaction schemes, the most important step toward the production of metal chalcogenide is the metal-to-phosphorus charge transfer shown in Scheme 1c. Although this charge-transfer process occurs at very high energy, [ME + TOPE + H]$^+$ is observed in the primary dissociations of [Cd + 2TOPS]$^{2+}$, [Zn + 2TOPS]$^{2+}$, and [Cd + 2TOPSe]$^{2+}$ as well as the secondary dissociations of [Cd + 3TOPO]$^{2+}$ and [Zn + 3TOPO]$^{2+}$.

Implications to TOPO-Based Nanocrystal Synthesis. TOPO is widely used as a strongly coordinating solvent for colloidal synthesis of nanocrystals.[6−9,12−18] TOPO allows size-controlled growth of nanocrystals to yield narrow emission.[6] In TOPO-based II−VI semiconductor nanocrystal synthesis, both TOPS and TOPSe are frequently used as chalcogen precursors, while dialkylcadmium and -zinc are used as metal precursors.[6,12−15,21] The present study shows that the metal−TOPO binding energy is much greater than both the metal−TOPS and −TOPSe binding energies for both cadmium and zinc, which implies that nanocrystals are primarily covered with TOPO during colloidal synthesis. The cone-shaped TOP having a 19 Å diameter base keeps other TOPE from coming closer to the TOPO-covered nanocrystal surface by exerting steric hindrance. TOPS or TOPSe compete with TOPO for binding to the metal

SCHEME 1: Intramolecular Reactions of [M + 2TOPE]$^{2+}$

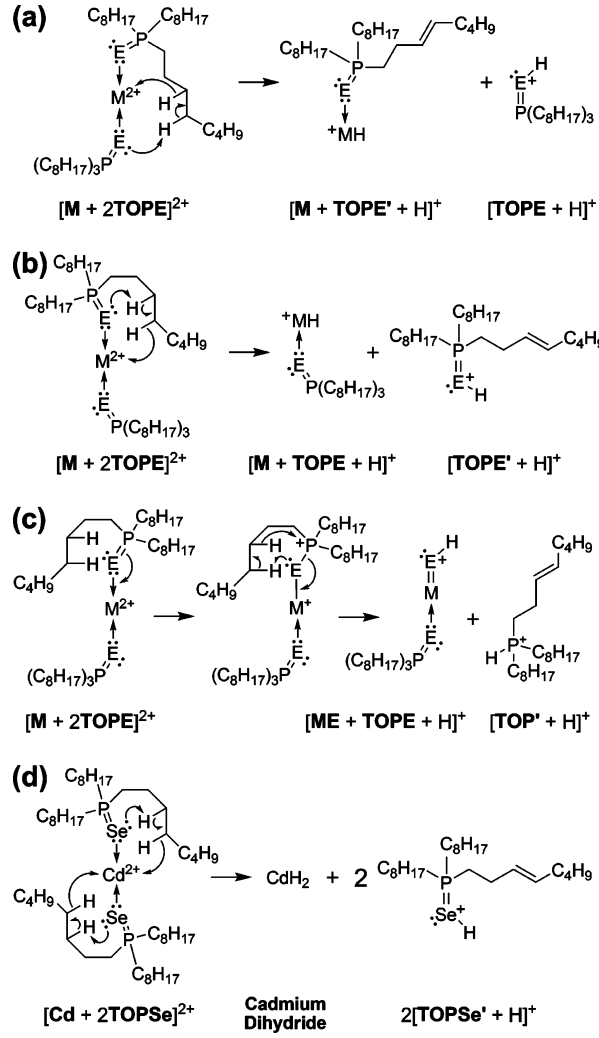

on the surface. Hence, once in a while, TOPO is replaced with TOPS or TOPSe on the nanocrystal surface, then TOPS or TOPSe can get closer to the metal ion to undergo metal-to-phosphorus charge transfer and result in the metal−chalcogenide formation with a release of TOP. It seems that the growth of nanocrystal is sterically controlled by TOPO and the growth rate is limited by the net flux of TOPS or TOPSe coming onto the surface sterically hindered by TOP. Although the TOPO-based synthesis employs highly reactive precursors like dialkyl metals, it requires a reaction temperature in the range of 300−350 °C,[6] which is much higher than the typical temperature range of 200−250 °C needed in TOPO-free syntheses employing more stable precursors such as metal carboxylates or phosphonates. Moreover, as the ratio of fatty acids or amines increases, the growth rate also increases in TOPO-based nanocrystal synthesis,[8,15] implying that less bulky ligands in place of TOPO facilitate the nanocrystal growth by removing a steric screen that limits an influx of TOPE onto the nanocrystal surface.

Conclusion

Collision-induced dissociation of [M + nTOPE]$^{2+}$ (M = Cd and Zn; E = O, S, and Se; n = 2−4) reveals the relative stabilities of metal−TOPE complexes. When the metal center is coordinatively unsaturated with n = 2−3, the zinc complexes

are more stable than the cadmium complexes for all three TOPEs. On the other hand, when the metal center is coordinatively saturated with $n = 4$, the zinc complexes are almost comparable to, but less stable than, the cadmium complexes due to steric hindrance by bulky TOP. Of the TOPEs, TOPO binds most strongly to the metal ion, whereas TOPSe does most weakly. The metal−TOPO binding energy is much greater than both the metal−TOPS and metal−TOPSe binding energies. The coordinatively saturated tetra-TOPE complexes lose TOPE exclusively upon collisional activation, whereas the coordinatively unsaturated di- and tri-TOPE complexes undergo intramolecular reactions, especially when the metal−TOPE binding energy is greater than activation barriers for rearrangements. It appears that metal hydride is formed at low energy and metal chalcogenide is formed at high energy. The formation of metal chalcogenide (sulfide and selenide) starts from the coordinatively unsaturated di-TOPE (E = S and Se) complexes, where the chalcogen atom can get closer to the metal center to initiate metal-to-phosphorus charge transfer. In TOPO-based colloidal synthesis of nanocrystals, it seems that TOPO is always covered on the surface and limits the influx of TOPS or TOPSe to the reactive metal center by placing a steric screen.

Acknowledgment. W.J.M. and S.J. contributed equally to this work and should be considered as joint first authors. We thank the support from Nano Research and Development Program through the Korea Science and Engineering Foundation funded by the Ministry of Education, Science, and Technology (Grant No. 2008-04540).

References and Notes

(1) Kamat, P. V. *J. Phys. Chem. C* **2008**, *112*, 18737–18753.
(2) Rogach, A. L.; et al. *Angew. Chem., Int. Ed.* **2008**, *47*, 6538–6549.
(3) Shin, S. K.; Yoon, H.-J.; Jung, Y. J.; Park, J. W. *Curr. Opin. Chem. Biol.* **2006**, *10*, 423–429.
(4) Medintz, I. L.; Uyeda, H. T.; Goldman, E. R.; Mattoussi, H. *Nat. Mater.* **2005**, *4*, 435–446.
(5) Michalet, X.; Pinaud, F. F.; Bentolila, L. A.; Tsay, J. M.; Doose, S.; Li, J. J.; Sundaresan, G.; Wu, A. M.; Gambhit, S. S.; Weiss, S. *Science* **2005**, *307*, 538–544.
(6) Murray, C. B.; Norris, D. J.; Bawendi, M. G. *J. Am. Chem. Soc.* **1993**, *115*, 8706–8715.
(7) Trindade, T.; O'Brien, P.; Zhang, X. *Chem. Mater.* **1997**, *9*, 523–530.
(8) Qu, L.; Peng, Z. A.; Peng, X. *Nano Lett.* **2001**, *1*, 333–337.
(9) Mohamed, M. B.; Tonti, D.; Al-Salman, A.; Chemseddine, A.; Chergu, M. *J. Phys. Chem. B* **2005**, *109*, 10533–10537.
(10) Deng, Z.; Cao, L.; Tang, F.; Zou, B. *J. Phys. Chem. B* **2005**, *109*, 16671–16675.
(11) Yang, Y. A.; Wu, H.; Williams, K. R.; Cao, Y. C. *Angew. Chem., Int. Ed.* **2005**, *44*, 6712–6715.
(12) Hines, M. A.; Guyot-Sionnest, P. *J. Phys. Chem.* **1996**, *100*, 468–471.
(13) Dabbousi, B. O.; Rodriguez-Viejo, J.; Mikulec, F. V.; Heine, J. R.; Mattoussi, H.; Ober, R.; Jensen, K. F.; Bawendi, M. G. *J. Phys. Chem. B* **1997**, *101*, 9463–9475.
(14) Peng, X.; Schlamp, M. C.; Kadavanich, A. V.; Alivisatos, A. P. *J. Am. Chem. Soc.* **1997**, *119*, 7019–7029.
(15) Talapin, D. V.; Rogach, A. L.; Kornowski, A.; Haase, M.; Weller, H. *Nano Lett.* **2001**, *1*, 207–211.
(16) Reiss, P.; Bleuse, J.; Pron, A. *Nano Lett.* **2002**, *2*, 781–784.
(17) Mekis, I.; Talapin, D. V.; Kornowski, A.; Haase, M.; Weller, H. *J. Phys. Chem. B* **2003**, *107*, 7454–7462.
(18) Talapin, D. V.; Mekis, I.; Götzinger, S.; Kornowski, A.; Benson, O.; Weller, H. *J. Phys. Chem. B* **2004**, *108*, 18826–18831.
(19) Li, J. J.; Wang, Y. A.; Guo, W.; Keay, J. C.; Mishima, T. D.; Johnson, M. B.; Peng, X. *J. Am. Chem. Soc.* **2003**, *125*, 12567–12575.
(20) Lim, S. J.; Chon, B.; Joo, T.; Shin, S. K. *J. Phys. Chem. C* **2008**, *112*, 1744–1747.
(21) Peng, X.; Manna, L.; Yang, W.; Wickham, J.; Scher, E.; Kadavanich, A.; Alivisatos, A. P. *Nature* **2000**, *404*, 59–61.
(22) Jun, Y.; Lee, S.-M.; Kang, N.-J.; Cheon, J. *J. Am. Chem. Soc.* **2001**, *123*, 5150–5151.
(23) Yu, W. W.; Wang, Y. A.; Peng, X. *Chem. Mater.* **2003**, *15*, 4300–4308.
(24) Milliron, D. J.; Hughes, S. M.; Cui, Y.; Manna, L.; Li, J.; Wang, L.-W.; Alivisatos, A. P. *Nature* **2004**, *430*, 190–195.
(25) Zhong, X.; Han, M.; Dong, Z.; White, T. J.; Knoll, W. *J. Am. Chem. Soc.* **2003**, *125*, 8589–8594.
(26) Zhong, X.; Feng, Y.; Knoll, W.; Han, M. *J. Am. Chem. Soc.* **2003**, *125*, 13559–13563.
(27) Protière, M.; Reiss, P. *Small* **2007**, *3*, 399–403.
(28) Fenn, J. B.; Mann, M.; Meng, C. K.; Wong, S. F.; Whitehouse, C. M. *Science* **1989**, *246*, 64–71.
(29) Loo, J. A. *Int. J. Mass Spectrom.* **2000**, *200*, 175–186.
(30) Gaumet, J. J.; Khitrov, G. A.; Strouse, G. F. *Nano Lett.* **2002**, *2*, 375–379.
(31) Arl, D.; Aubriet, F.; Gaumet, J. J. *J. Mass Spectrom.* **2009**, *44*, 763–771.
(32) Jones, J. L.; Dongré, A. R.; Somogyi, Á.; Wysocki, V. H. *J. Am. Chem. Soc.* **1994**, *116*, 8368–8369.
(33) Wan, K. X.; Gross, M. L.; Shibue, T. *J. Am. Soc. Mass Spectrom.* **2000**, *11*, 450–457.
(34) Daniel, J. M.; Friess, S. D.; Rajagopalan, S.; Wendt, S.; Zenobi, R. *Int. J. Mass Spectrom.* **2002**, *216*, 1–27.
(35) David, W. M.; Brodbelt, J. S. *J. Am. Soc. Mass Spectrom.* **2003**, *14*, 383–392.
(36) Oxtoby, D. W.; Gillis, H. P.; Nachtrieb, N. H. *Principles of Modern Chemistry*, 5th ed.; Thompson Brooks/Cole: Belmont, CA, 2002.
(37) Carson, R. R.; Meek, D. W. *Inorg. Chem.* **1974**, *13*, 1741–1747.
(38) Byrd, H. C. M.; Guttman, C. M.; Ridge, D. P. *J. Am. Soc. Mass Spectrom.* **2003**, *14*, 51–57.

JP905153V